micro

MDPI

Article

Matrix Effect of Properties of Au, ZnO and Eu_2O_3: Silica, Titania and Alumina Matrices

Carlos Díaz [1], Olga Cifuentes-Vaca [2] and María Luisa Valenzuela [3,*]

[1] Departamento de Química, Facultad de Química, Universidad de Chile, La Palmeras 3425, Nuñoa, Casilla 653, Santiago 7750000, Chile; cdiaz@uchile.cl
[2] Facultad de Ciencias Exactas, Universidad Andrés Bello, Sede Concepción, Autopista Concepción-Talcahuano 7100, Talcahuano 4260000, Chile; ocifuentes@unab.cl
[3] Grupo de Investigación en Energía y Procesos Sustentables, Facultad de Ingeniería, Instituto de Ciencias Aplicadas, Universidad Autónoma de Chile, Av. El Llano Subercaseaux 2801, Santiago 8900000, Chile
* Correspondence: maria.valenzuela@uautonoma.cl

Abstract: The composites Au/SiO_2, Au/TiO_2, Au/Al_2O_3, ZnO/TiO_2, ZnO/TiO_2, ZnO/Al_2O_3 and Eu_2O_3/SiO_2, Eu_2O_3/TiO_2 and Eu_2O_3/Al_2O_3 were prepared using a solid-state method. The effect of the polymer precursors was investigated using two precursor polymers, Chitosan and Poly(styrene-co-4vinylpyridine), (PS-co-4-PVP) in the M/M_xL_y•Chitosan//$M'_xO'_y$ as well as M/M_xL_y•PS-co-4-PVP//$M'_xO'_y$ with $M'_xO'_y$ = SiO_2, TiO_2 and Al_2O_3. The effects on the particle size and morphology were observed. The new composites were characterized using X-ray powder diffraction, SEM-EDS mapping and HRTEM analysis. The distribution of the metallic nanoparticles as well as the metal oxide nanoparticles inside the matrices depend on the matrix. Marked optical and photocatalytic effects of the Au, ZnO and Eu_2O_3 inside the SiO_2, TiO_2 and Al_2O_3 matrices are expected. An experiment is in course.

Keywords: composites; solid-state method; photocatalytic effect

check for updates

Citation: Díaz, C.; Cifuentes-Vaca, O.; Valenzuela, M.L. Matrix Effect of Properties of Au, ZnO and Eu_2O_3: Silica, Titania and Alumina Matrices. *Micro* **2023**, *3*, 699–714. https://doi.org/10.3390/micro3030049

Academic Editor: Ewa Kowalska

Received: 6 June 2023
Revised: 11 August 2023
Accepted: 16 August 2023
Published: 19 August 2023

1. Introduction

Some of the typical properties of nanostructured nanoparticles such as the plasmon, their size, their morphology and band gap depend on the media that surround them [1,2]. For nanoparticles in a solution, their stabilizer and solvents control and/or affect these properties [1,2]. In a solid state, when these nanoparticles are inside of a solid matrix, those properties are affected by the characteristic of the matrix. Scarce studies of the medium on the optical effects and on other properties have been reported, with almost all of them using metallic nanoparticles [2–4], and no studies with metal oxide nanoparticles have been reported. For solid states, the optical properties of metal nanoparticles (Au, Ag, and Cu) are greatly influenced by the interface between the nanoparticles and the matrix [1,3,4]. The influence of the structure's environment on the optical properties of some metal noble nanoparticles were recently revised by Tondello and Parkin [3,4]. Matsuoka [5] studied the influences of the dielectric constant of TiO_2, ZrO_2 and Al_2O_3 on the optical properties of Au nanoparticles. A direct linear relation between the maxima absorption of the Au nanoparticles with the dielectric constant was found. On the other hand, a solution study of the external dielectric medium (of the solvent) on the surface plasmon resonance spectrum of silver nanoparticles, from an experimental approach as well as a theoretical approach, was reported by Schatz et al. [1,2]. A theoretical study of the influences of the size, shape and dielectric environment on the optical properties of metal nanoparticles in a solution was reported by Schatz et al. [1]. Saviot [6] studied the optical properties of gold and silver inside an alumina matrix. Goutam De [7] studied the optical properties of the nanoclusters of Cu inside silica. Additionally, Torrell studied the functional and optical properties of

Au:TiO_2 nanocomposite films [8]. A direct relation between the size of the Au particles and the annealing temperature was found.

Finally, Mattei et al. [9] reported the effect of the ZrO_2•SiO_2 matrix on the optical properties of silver-doped ZrO_2. Although the composites M/M'_xO' have been studied the most, the composites $M_xO_y/M'_xO'_y$ have been scarcely investigated [10–12].

Previously, we studied the matrix effect of the medium effect of NiO on the optical properties and catalytic degradation of methylene blue inside the matrices SiO_2, TiO_2 and Al_2O_3 [13]. The efficiency of the photocatalytic activity depends on the formation of a p-n junction between NiO acting as p-NiO and the metal oxide matrix acting as an n-metal oxide. TiO_2 presents the most effective p-NiO//n-TiO_2 junction. Moreover, the optical parameters Eg and λ_{max} depend on the dielectric constant and the refractive index of the matrix medium, in a manner of which depends on the preparation procedure [13].

Now, we report the synthesis and characterization of the nanocomposites Au/SiO_2 [14], Au/TiO_2, Au/Al_2O_3, ZnO/SiO_2 [15], ZnO/TiO_2, ZnO/Al_2O_3, Eu_2O_3/SiO_2, Eu_2O_3/TiO_2 and Eu_2O_3/Al_2O_3 [16] for a future study of the optical as well as photocatalytic properties of Au, ZnO and Eu_2O_3 inside SiO_2, TiO_2 and Al_2O_3 matrices. We selected Au as a typical noble metal, ZnO as a typical metal oxide and Eu_2O_3 as a typical representative of the lanthanide series. As a preparative general method for these composites, we used the solid-state method from the pyrolysis of the precursors M_xL_y•Chitosan//$M'_xO'_y$, where M_xL_y = $AuCl_3$, $ZnCl_2$ and $Eu(NO_3)_3$ and $M'_xO'_y$ = SiO_2, TiO_2 and Al_2O_3, using a general previously reported method [13–18]. Some preliminary reports of Au/SiO_2 [14], ZnO/SiO_2 [15], Eu_2O_3/SiO_2 [16], ReO_3/SiO_2 [17], Rh/RhO_2/SiO_2 [18], Rh_2O_3/SiO_2 [18], ThO_2/SiO_2 and ThO_2/TiO_2 [19] have recently been reported. A general schematic diagram of the method is shown in Figure 1.

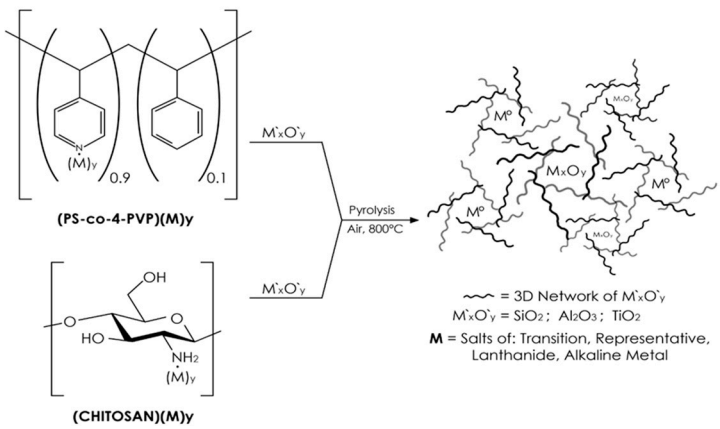

Figure 1. General representation of the formation of the nanocomposites $M_xO_y/M'_xO'_y$.

2. Materials and Methods

The composites were prepared according to a previously reported method [13–18]. Some experimental details used for the preparation of the composites Au//$M'_xO'_y$, ZnO//$M'_xO'_y$ and Eu_2O_3//$M'_xO'_y$ are shown in Supplementary Information S1.

2.1. Materials and Common Procedures

$AuCl_3$, $ZnCl_2$ and $Eu(NO_3)_3$ from Aldrich (Sigma-Aldrich Quimica Ltda, Chile) were used as received. Chitosan (Aldrich) of low molecular weight was used as received. An estimation of the molecular weight was performed via viscosimetry. The average molecular weight was determined using the Mark–Houwink equation, and values of [h] were obtained using the parameter previously reported by Rinaudi et al. [20]. The solvent used was an aqueous solution of acetic acid, NaCl and urea. The value was Mw = 61.000. All the reactions were made in CH_2Cl_2 as solvent. Poly(styrene-co-4vinylpyridine) (Aldrich) with 90% of pyridine groups was used as received.

2.2. General Procedure

Metal macromolecular complexes (1)–(18) were prepared according to published procedures [13–18]. In a typical synthesis, the respective metallic salt was added in a Schlenk tube over a CH_2Cl_2 solvent under magnetic stirring and then the respective polymer PSP-co-4-PVP or Chitosan was added according to a 1:1 molar ratio. The reaction time and other details for each metallic salt's reaction are given in Table S1 of the Supplementary Information. After this, the supernatant solution (if the solid decanted) was extracted with a syringe, and the solid was dried under a reduced pressure. Further experimental details for the reactions are given in Table S1 of the Supplementary Information. Owing to their insolubility, the characterization of the precursors was made only via IR spectroscopy.

2.3. Pyrolysis of the Precursors

The pyrolysis experiments were made by pouring a weighed portion (0.05–0.15 g) of the metal polymer precursor 1–18 into aluminum oxide boats that were placed in a furnace (Daihan oven model Wise Therm FHP-12) under a flow of air, heating from 25 °C to upper temperature limits of 300 °C, and then to 800 °C, followed by annealing for 2–4 h in each case. The heating rate was consistently maintained at 10 °C min^{-1} for all experiments. Solid pyrolytic samples were characterized via X-ray diffraction of powders (XRD), scanning electron microscopy (SEM), high-resolution transmission electron microscopy (HRTEM) and Fourier transform infra-red (FTIR) spectroscopy. SEM images were acquired with a Philips EM 300 scanning electron microscope. Energy dispersive X-ray analysis (EDAX) was performed on a NORAN Instrument micro-probe attached to a JEOL 5410 scanning electron microscope. TEM data were acquired using a JEOL SX100 and a JEOL 2011 transmission electron microscope. High-resolution transmission electron microscopy (HR-TEM) was performed using a JEOL 2000FX TEM microscope at 200 kV to determine the average particle size, distribution, elemental composition and crystallinity of the samples. The average particle size was calculated using the Digital Micrograph software. The TEM samples were prepared by dispersing pyrolyzed material onto copper grids and dried at room temperature. X-ray diffraction (XRD) was conducted at room temperature on a Siemens D-5000 diffractometer with θ–2θ geometry. The XRD data were collected using Cu-Kα radiation (40 kV, 30 mA). FTIR measurements were performed on a Perkin Elmer FTIR spectrophotometer, Spectrum BXII model.

3. Results and Discussions

The composites Au/SiO_2, Au/TiO_2, Au/Al_2O_3, ZnO/TiO_2, ZnO/TiO_2, ZnO/Al_2O_3 and Eu_2O_3/SiO_2, Eu_2O_3/TiO_2 and Eu_2O_3/Al_2O_3 were identified via power XRD diffraction. The composite Au/SiO_2 was previously studied in [14]. For Au/TiO_2 (see Supplementary Information S2), the main diffraction peaks of the Au of planes (111), (200), (2201) and (311) were clearly observed [14], as well as the main diffraction peaks of the matrix TiO_2 in the anatase of planes (101), (004), (220), (105) and (211) [13]. For the Au/TiO_2 obtained from the PS-co-4-PVP precursors, a similar XRD diffraction pattern was observed (see Supplementary Materials). For Au/Al_2O_3, the diffraction pattern shows the main diffraction peaks of the Au of planes (111), (200), (2201) and (311) [14], and shows less intense main diffraction peaks of the matrix Al_2O_3 for planes (014), (110), (300), (105) and (119) [13] (see Supplementary Information S2). A similar XRD diffraction pattern was observed for Au in the Au/Al_2O_3 composite in addition to the diffraction pattern of Al_2O_3 (indicated in the XRD pattern) from the Chitosan as well as the PS-co-4-PVP container precursors (see also Supplementary Information S2). For ZnO/TiO_2 from the Chitosan, weak peaks of ZnO from planes (100), (002), (103) and (201) [15] were observed. On the other hand, strong diffraction peaks from planes (101), (103), (200), (105), (211) and (215) of the TiO_2 anatase were observed. A similar XRD diffraction pattern was observed for the ZnO/TiO_2 composite from the PS-co-4-PVP precursors. For the ZnO/Al_2O_3 composite from the Chitosan precursors, strong diffraction peaks from planes (100), (002), (102) and (103) assigned to ZnO are present in their XRD patterns [15]. On the other hand, weak diffraction peaks

assigned to planes (014), (110), (300), (105) and (116) of Al_2O_3 were also observed [13]. A similar XRD pattern from the ZnO/Al_2O_3 composite from the PS-co-4-PVP polymer was observed. For the Eu_2O_3/TiO_2 composite from Chitosan, an intense plane (211), as well as weak peaks corresponding to planes (123), (411), (600), (543), and (642) of Eu_2O_3, were observed [16]. On the other hand, for Eu_2O_3/TiO_2 from PS-co-4-PVP, a similar XRD pattern was observed. For the Eu_2O_3/Al_2O_3 from Chitosan, owing to the luminescence of the sample, the base line increased as the value of 2θ increased. Despite this, the typical peaks of Eu_2O_3 and Al_2O_3 were clearly observed (see Supplementary Information S2).

The HRTEM measurements were made for some representative M_xL_y•Chitosan//M_xO_y composites. According to the HRTEM analysis, for the Au/TiO_2 composite, the TiO_2 matrix induced the nucleation of uniform nanoparticles smaller than the Au/Al_2O_3 composite, and where the Au nanoparticles were bigger and more irregular, they were induced by the Al_2O_3 matrix (see Figure 2).

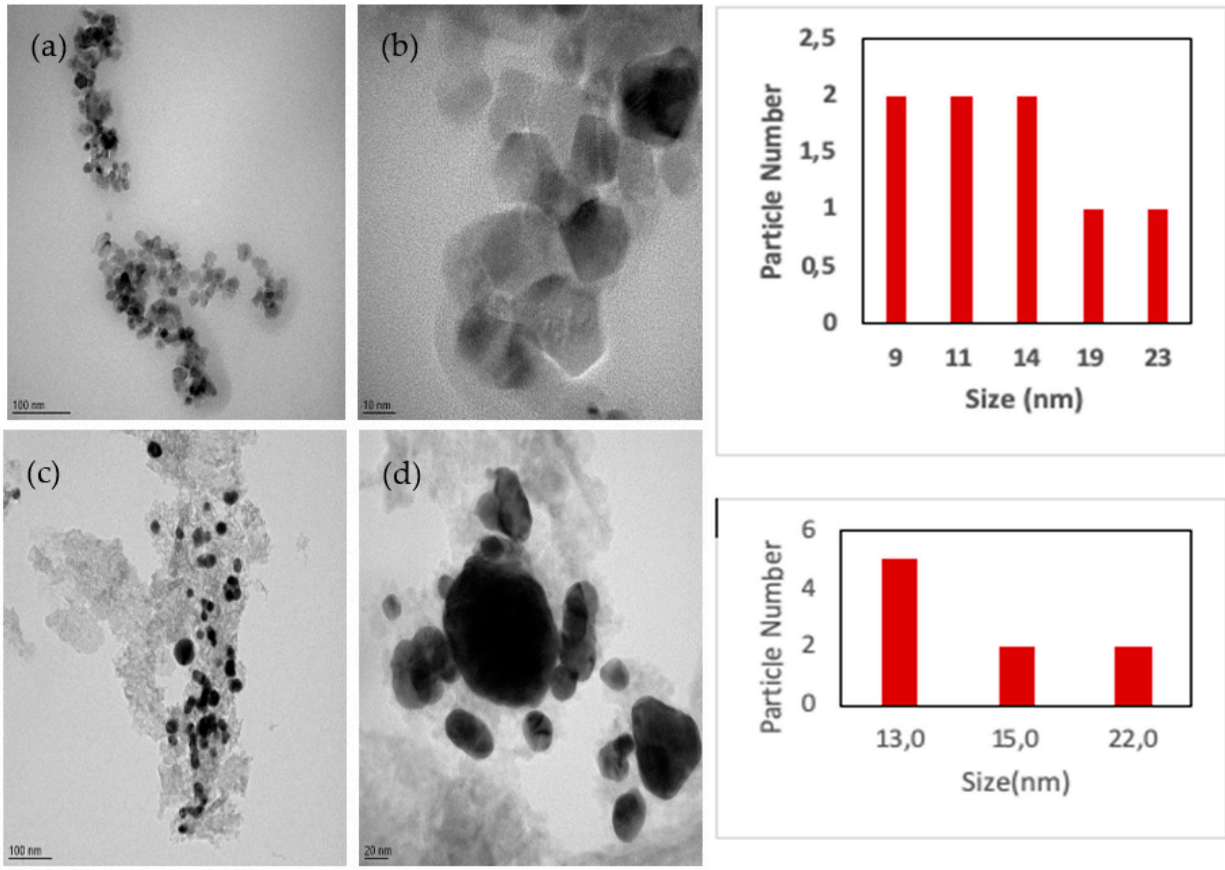

Figure 2. HRTEM of the composites Au/TiO_2 (**a**,**b**) and Au/Al_2O_3 (**c**,**d**) and their histogram.

On the other hand, for the ZnO/Al_2O_3 composite obtained from the Chitosan precursor, some polymorphological shapes were observed (see Figure 3). In addition, some squared and octahedron-shaped nanoparticles (enclosed in red circles) as well as some lamellar areas were observed.

For Eu_2O_3/SiO_2 (see Figure 4), big shapes were observed, as shown in Figure 4.

As for the Eu_2O_3/TiO_2 nanoparticles (see Figure 5), big shapes of TiO_2 coated with Eu_2O_3 were observed. The EDS analysis shown in Figure 5b,c, confirms these features.

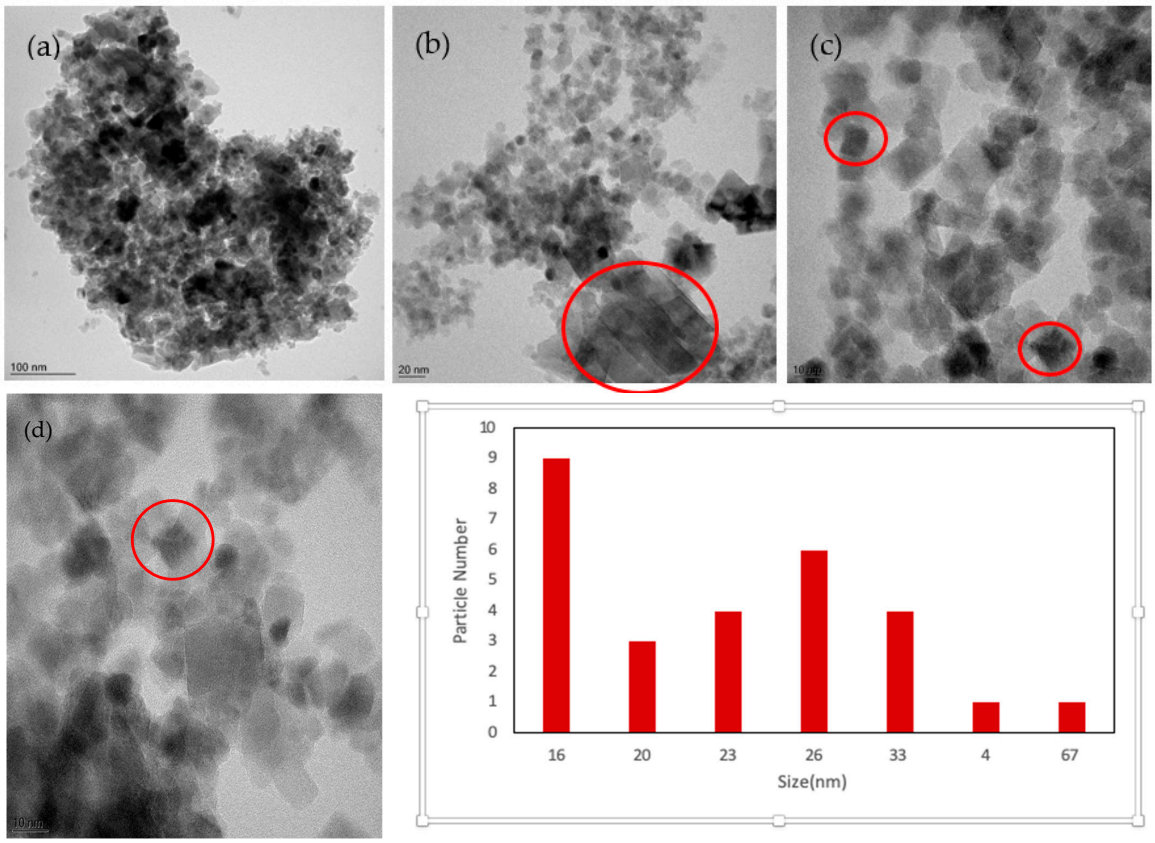

Figure 3. HRTEM of the composite ZnO/Al_2O_3 at different magnification (**a**–**d**) from Chitosan and their histogram.

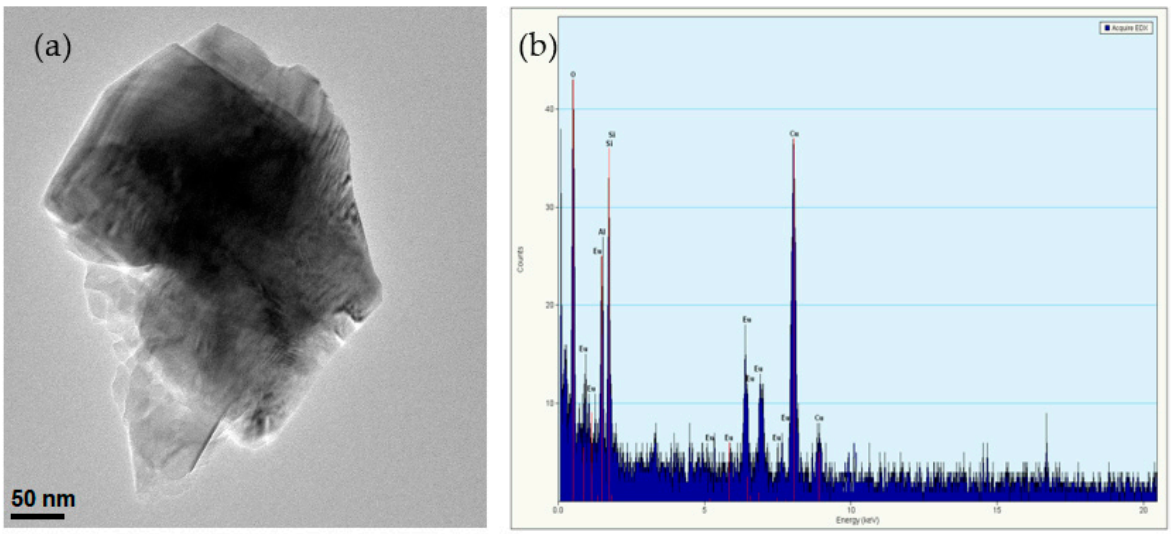

Figure 4. TEM image for Eu_2O_3/SiO_2 composite (**a**) and their EDS (**b**).

Also, in some areas, the nanoparticles of the TiO_2 anatase showing the typical interplanar 0.35 nm corresponding to the (101) plane were observed, as shown in Figure 6, which is in agreement with the findings from the XRD analysis.

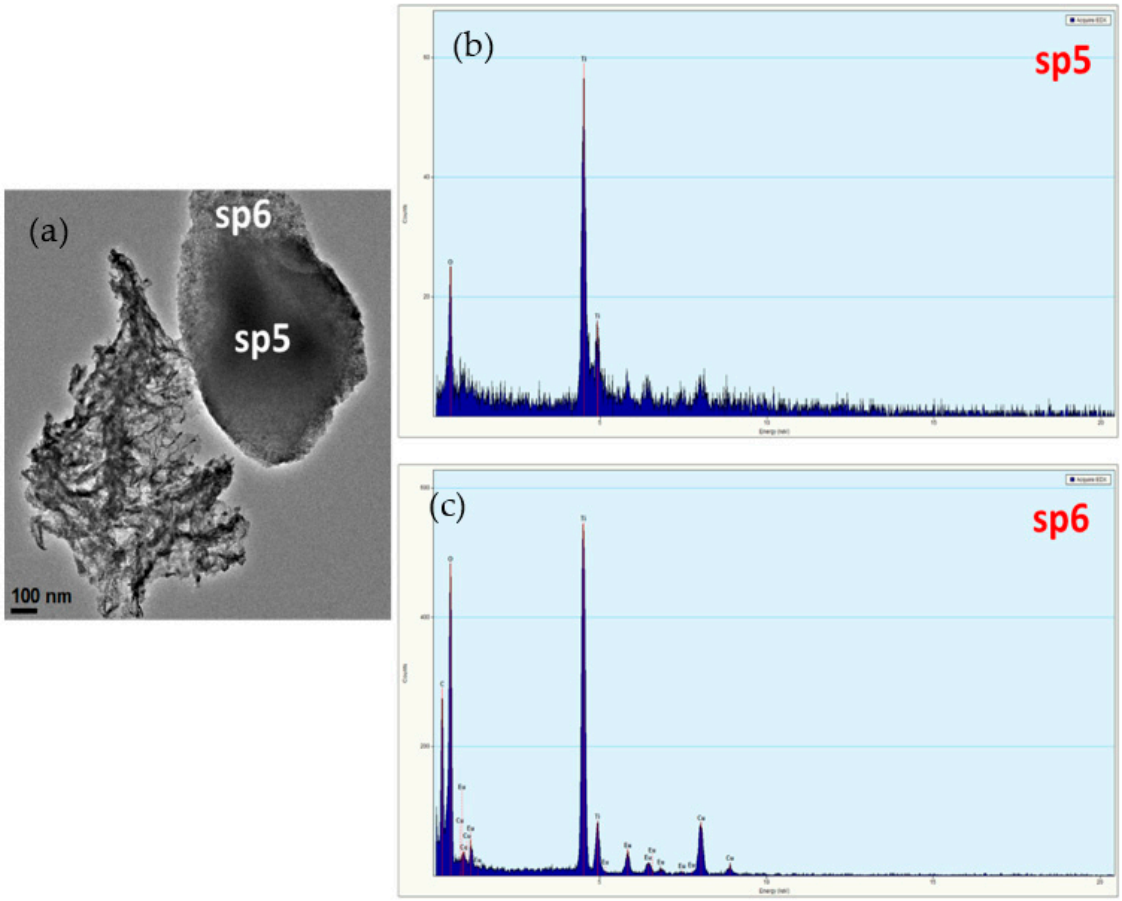

Figure 5. TEM image for Eu_2O_3/TiO_2 composite (**a**) and their EDS in two zones (**b**,**c**).

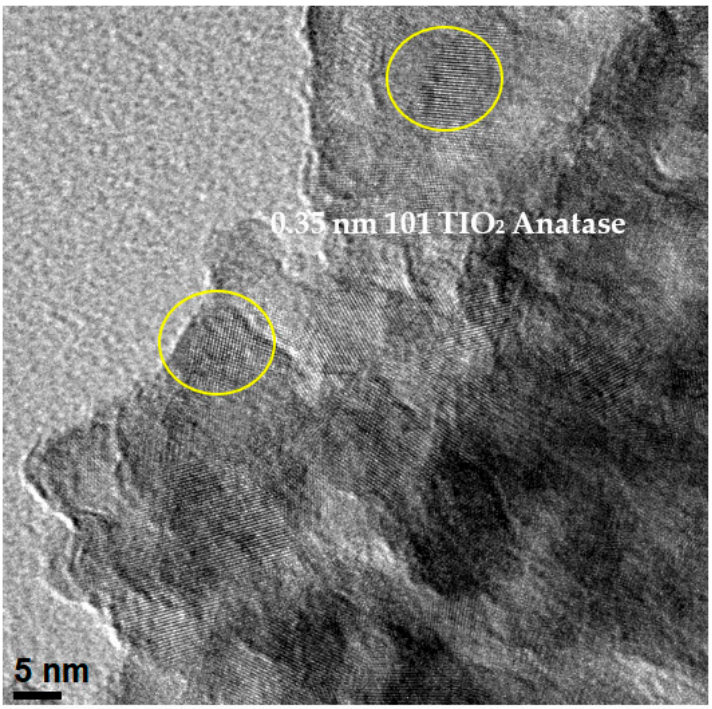

Figure 6. HRTEM image of Eu_2O_3/TiO_2 composite showing some TiO_2 anatase nanoparticles (yellow circle).

For the Eu_2O_3/Al_2O_3 composite, small "type worms" were observed (see Figure 7).

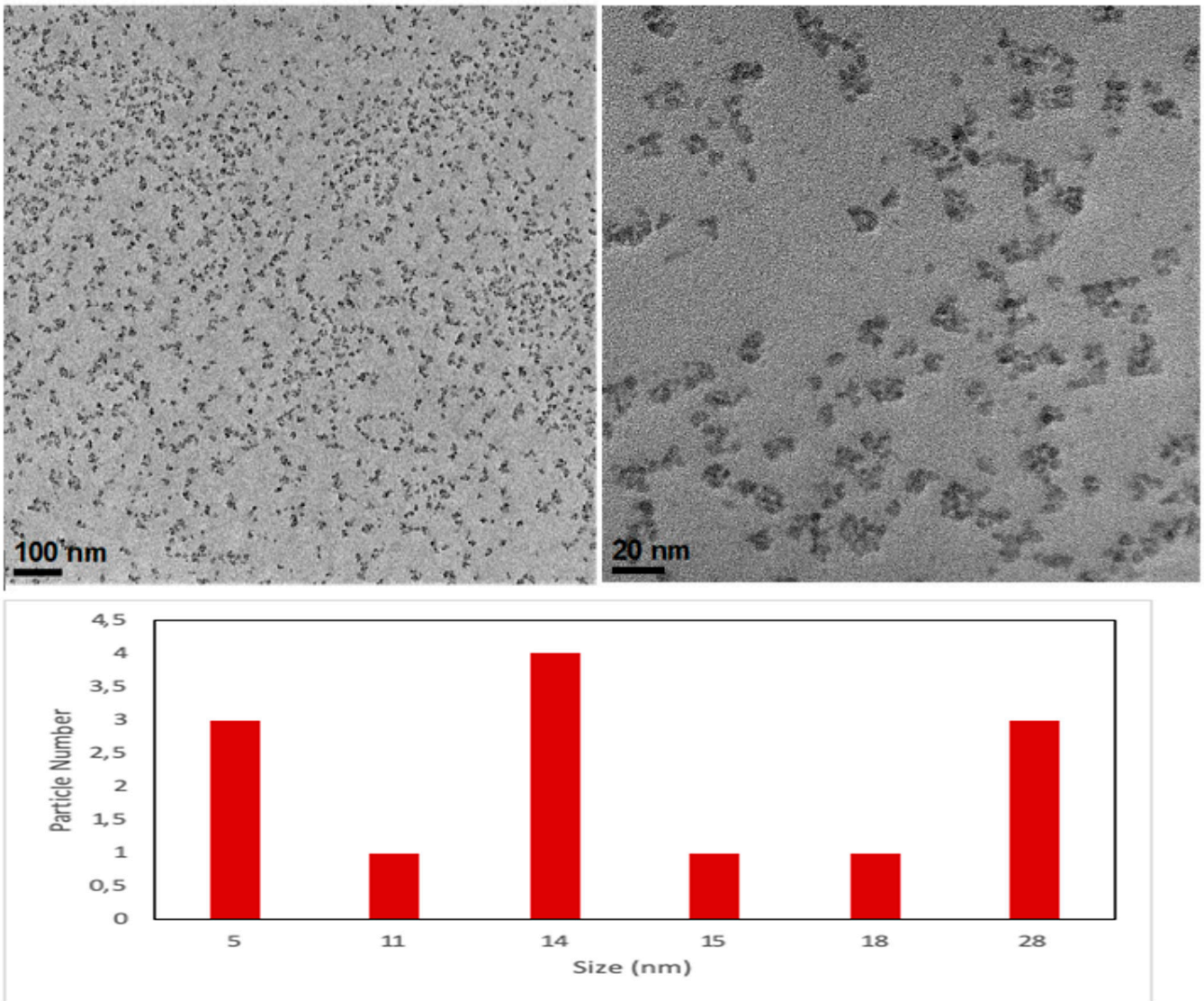

Figure 7. HRTEM image for the Eu_2O_3/Al_2O_3 composite and histogram.

For some of the composites, the distributions of the respective Au, ZnO and Eu_2O_3 inside the SiO_2, TiO_2 and Al_2O_3 matrices were investigated via SEM-EDS mapping. Well-dispersed and small Au nanoparticles were observed.

The SEM EDS mapping for the composite Au/SiO_2 was previously reported in [14] (see Supplementary Information S3).

For the composite Au/TiO_2, as shown in Figure 8, a homogeneous distribution of Au nanoparticles inside TiO_2 was observed.

For the composite Au/Al_2O_3, the distribution of the Au nanoparticles inside the Al_2O_3 matrix was not very homogeneous, and some agglomerations of the Au nanoparticles in some zones of the aluminum oxide matrix were observed (see Figure 9). Additionally, there appears to be a matrix effect of the dispersion of the Au nanoparticles inside the Al_2O_3 matrix.

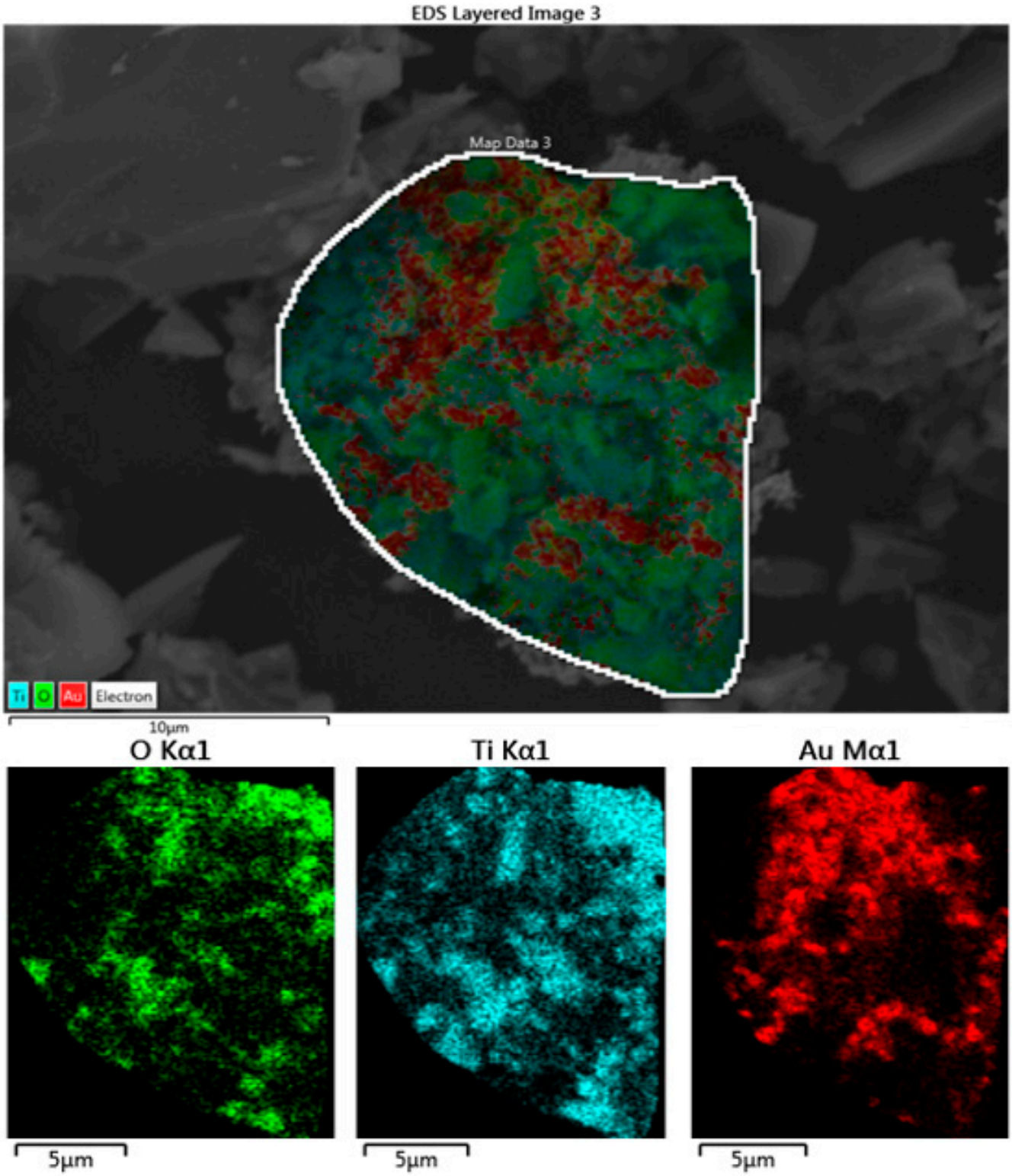

Figure 8. EDS mapping of Au/TiO_2 composite showing the distribution of the Au nanoparticles inside TiO_2.

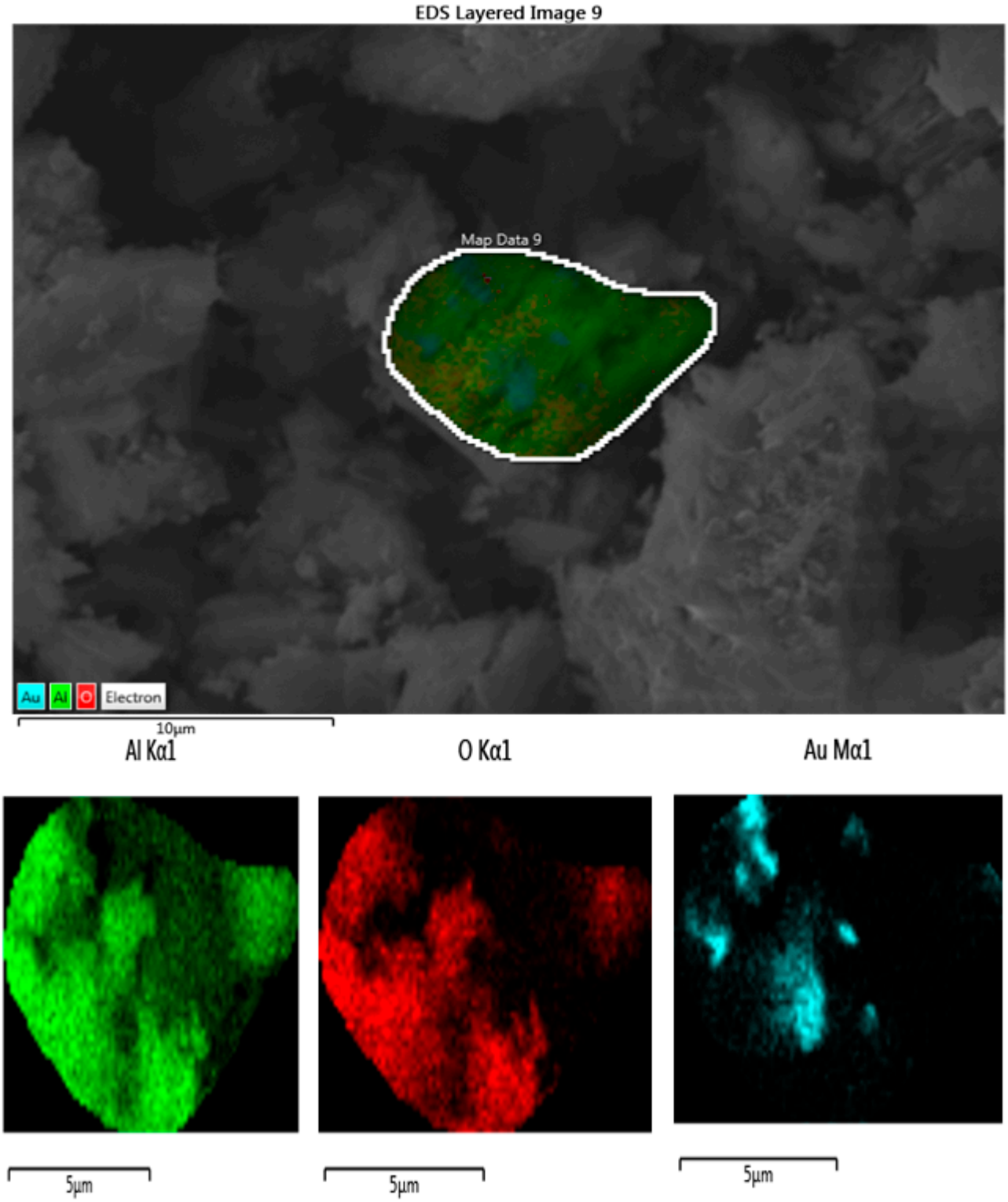

Figure 9. EDS mapping of Au/Al_2O_3 composite showing the distribution of the Au nanoparticles inside Al_2O_3.

On the other hand, for the composite ZnO/Al_2O_3, a near homogeneous distribution of the ZnO nanoparticles inside the Al_2O_3 matrix was observed (see Figure 10).

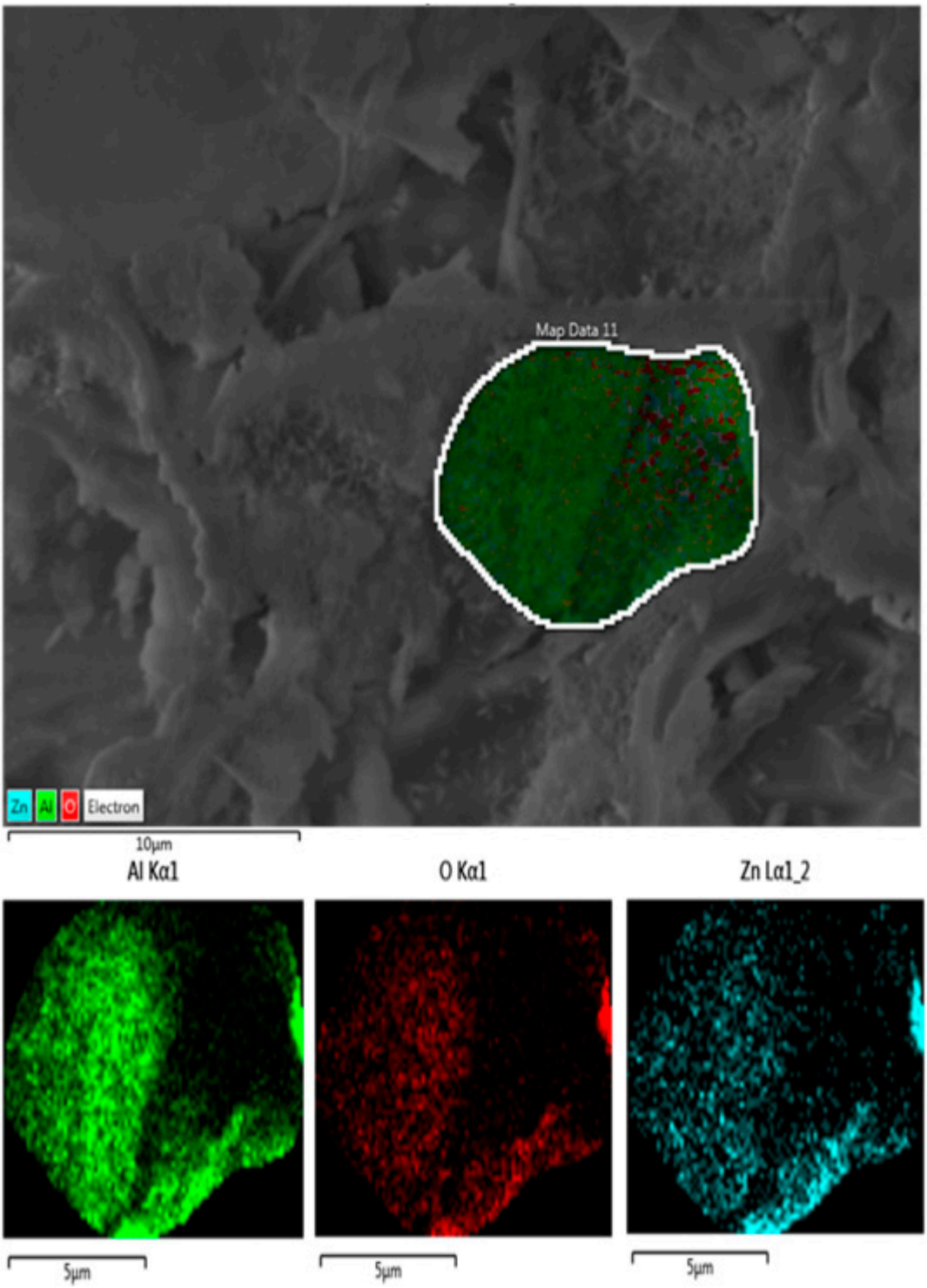

Figure 10. EDS mapping of ZnO/Al_2O_3 composite showing the distribution of the ZnO nanoparticles inside Al_2O_3.

For the Eu_2O_3/TiO_2 composite, a distribution of very abundant and small Eu_2O_3 nanoparticles inside TiO_2 was observed (see Figure 11).

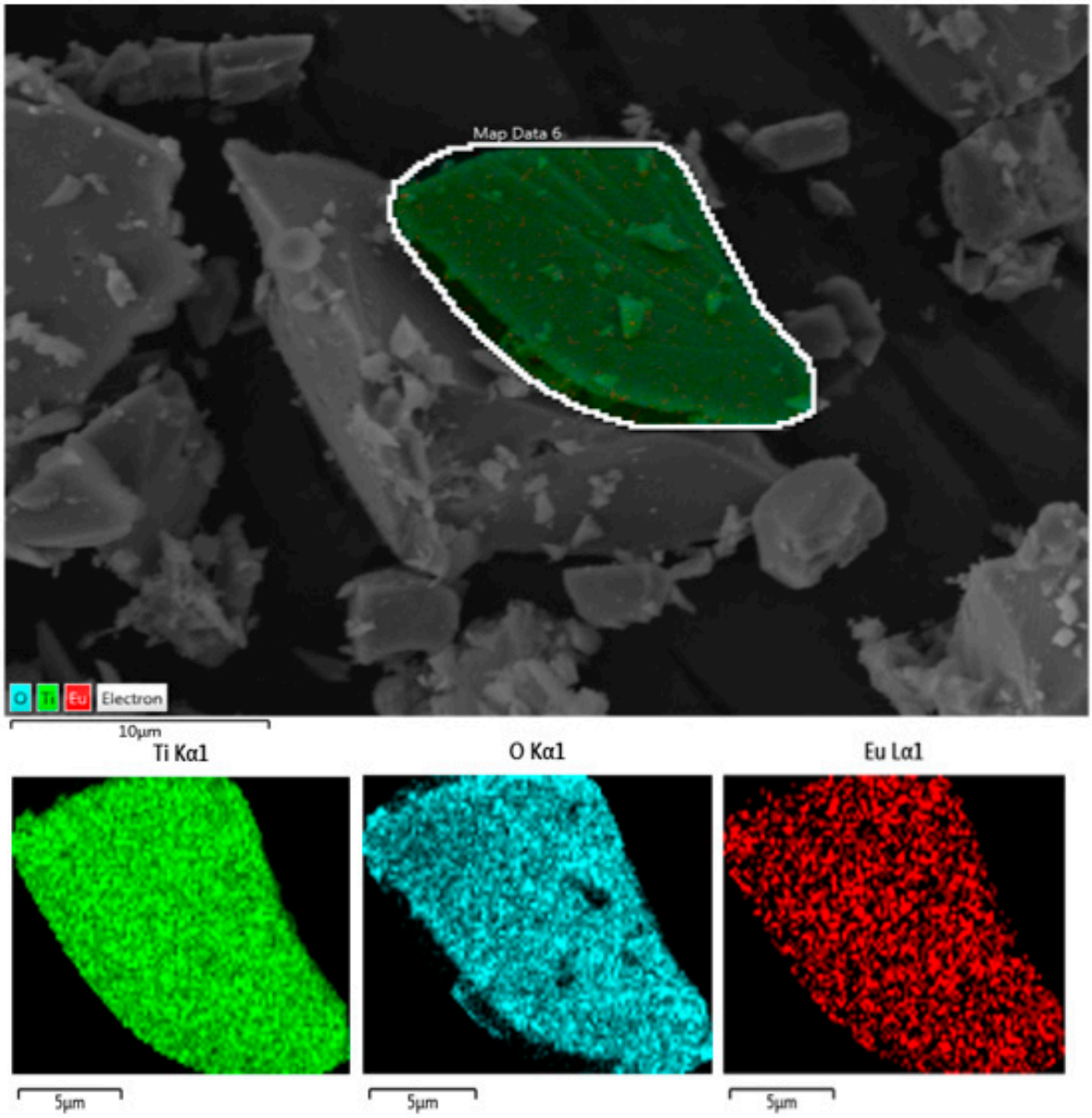

Figure 11. EDS mapping of the Eu_2O_3/TiO_2 composite showing the distribution of the Eu_2O_3 nanoparticles inside TiO_2.

On the other hand, for the Eu_2O_3/Al_2O_3 composite, a linear sweep study per element was performed. As shown in Figure 12, there are zones where the contents of oxygen and aluminum are high, and the Eu content is lower, suggesting the presence of a minor content of Eu_2O_3 inside the matrix Al_2O_3, but it would need to have a higher content to be in accordance with the behavior of Al_2O as a matrix.

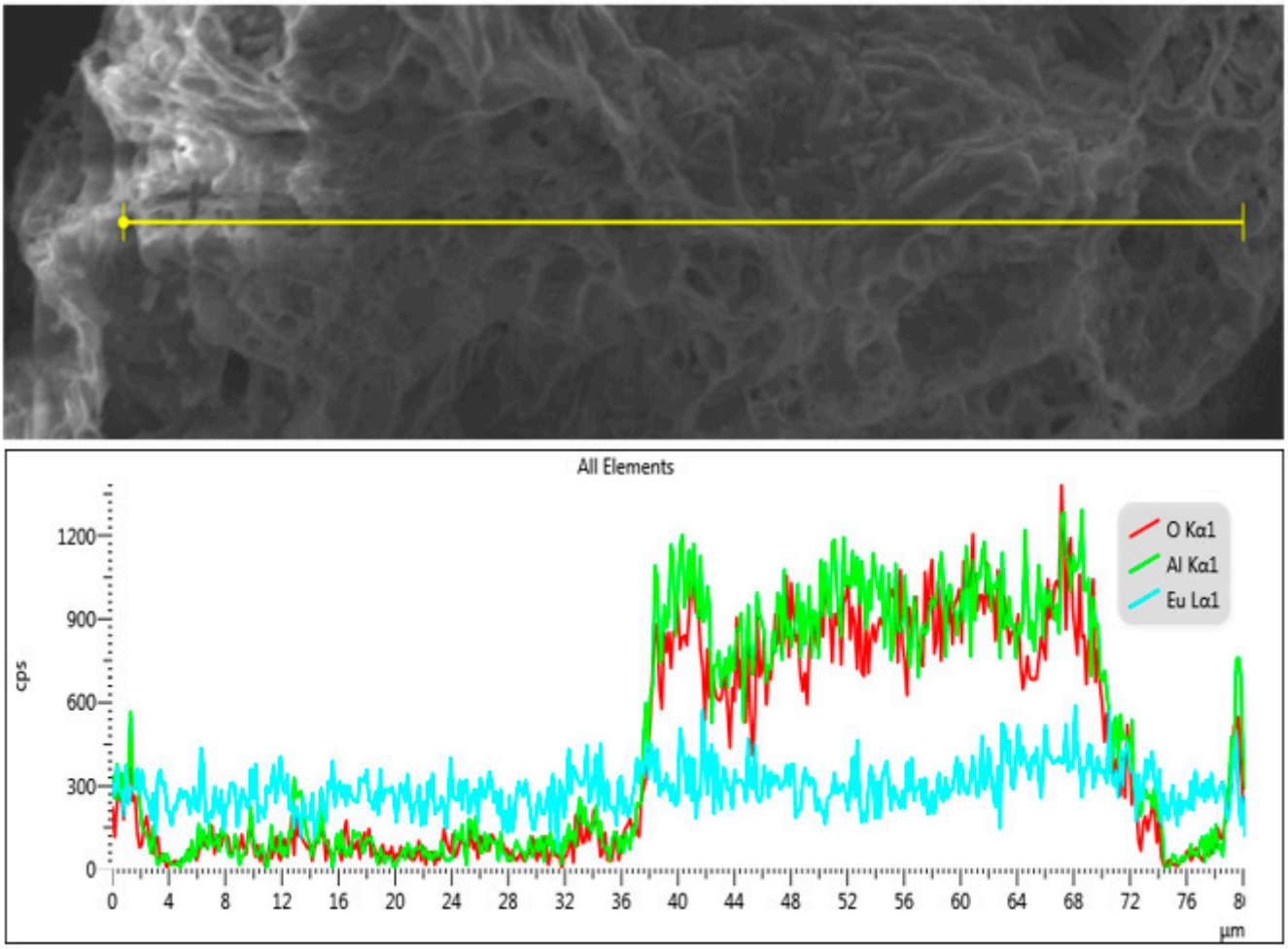

Figure 12. Linear sweep SEM EDS per element of the Eu_2O_3/Al_2O_3 composite.

3.1. Effect of the SiO_2, TiO_2 and Al_2O_3 Matrices on the Distribution of Au, ZnO and Eu_2O_3 inside Them

The SiO_2, TiO_2 and Al_2O_3 matrices influence the distribution of the Au, ZnO and Eu_2O_3 inside them. For Au included in SiO_2, a uniform distribution was observed (see Supporting Information S3). On the other hand, for the Au inside TiO_2, non-uniform nanoparticles and some agglomerate nanoparticles were observed (see Figure 8). For the Au nanoparticles inside Al_2O_3 and similar situations, see Figure 9.

For ZnO inside Al_2O_3, nanoparticles that were not well distributed and some agglomerate nanoparticles of the oxide inside alumina were observed (see Figure 10).

On the other hand, for Eu_2O_3 inside TiO_2, a uniform distribution but very close lanthanide oxide inside the matrix was observed (see Figure 11).

3.2. Morphology Effect of the Au, ZnO and Eu_2O_3 Nanoparticle by the Matrices SiO_2, TiO_2 and Al_2O_3

The SEM image of the Au nanoparticles included inside the SiO_2, TiO_2 and Al_2O_3 matrices shows some minor effect on the morphology, as shown in the Supporting Information (S4). For the Au inside SiO_2 and TiO_2, dense agglomerate grains with variated forms were observed, while for the Au inside Al_2O_3, a "some foam" 3D form was observed.

For the Eu_2O_3 nanoparticles, the inclusion inside the matrices TiO_2 and Al_2O_3 produces significant changes in their morphology, as shown in the Supporting Information (S5). For Eu_2O_3 inside TiO_2, dense grains of several shapes that were not distributed uniformly were observed. On the other hand, for Eu_2O_3 inside TiO_2, a "foam like" morphology was observed.

For the composite ZnO/Al_2O_3, a "foam type" morphology was observed, as shown in Supporting Information S6, which is formed by "worms", as shown in Supporting Information S6b, in the most enlarged image. A comparison with the morphology of the ZnO/SiO_2 was not possible because ZnO reacts with SiO_2 to give Zn_2SiO_4 and SiO_2 [15]. On the other hand, the study for the ZnO/TiO_2 composite is not available.

3.3. Morphology Comparation

3.3.1. Au

The morphology of the Au/SiO_2, Au/TiO_2 and Au/Al_2O_3 composites depends a lot on the preparation method used. For Au/SiO_2, rather large grains and agglomerates of various shapes in some areas were observed (see Supplementary Materials S4a), while for the Au/SiO_2 composite obtained from a PE-CVD/RF sputtering route, low-sized particles with a pseudo-spherical shape (cluster-like systems) were observed on the growth surface [21]. On the other hand, SiO_2/Au hybrid microspheres with a diameter of 200 nm were obtained via the galvanic replacement of SiO_2/Ag hybrid microspheres and chlorauric acid ($HAuCl_4$) solution [22]. Also, monodispersed nanospheres were obtained via a straightforward one-step method, which was developed to synthesize Au–SiO_2 composite nanospheres [23]. Monodisperse hybrid silica nanospheres that had anilino-methyl on the surfaces were prepared first. The as-prepared hybrid silica nanospheres were then used to obtain Au nanocrystal through the redox reaction of $HAuCl_4$ and anilino-methyl.

3.3.2. For Au/TiO_2 Composites

Using our current method in the solid state, Au/TiO_2 nanocomposites were obtained that present dense, separated grains of various sizes and shapes (see Supplementary Material S4b). On the other hand, for the Au/TiO_2 composites prepared using a spray hydrolytic method and using a photoreduction technique at 90 °C, non-uniform growth of particle size distribution in spherical morphology were observed. The particle size is in the range of 6.0–6.7 nm [24]. Using electrospinning combined with a calcination treatment, the Au/TiO_2 nanofiber composites were prepared [25].

3.3.3. Au/Al_2O_3

Using our solid-state method, a "foam" type morphology was observed (see Supplementary Material S4c), and $Au@Al_2O_3$ core–shell particles that were mostly spherical in shape with a conical cavity were obtained using a one-step method with continuous-wave fiber laser ablation on an aluminum (Al) plate coated with a gold (Au) monolayer immersed in ethanol [26]. The shape of the nanoparticles was roughly spherical with an average size of approximately 20 nm.

Spherical nanoporous forms of the Au/Al_2O_3 composite with sizes in the range of 54–293 nm were obtained via a combination of solid-state dewetting of Ag/Au bi-layers and subsequent dealloying [27]. The morphology seen by the SEM shows nanoporous spheres with pore sizes in the range of 11.6–50.4 nm.

3.3.4. ZnO/Al_2O_3

As can be seen from Figure S6 of the Supplementary Material, the SEM image shows a morphology of a mixture of "worm-like" shapes and continuous zones of metallic foams. This morphology contrasts with that obtained using a method in which the ZnO and Al_2O_3 sols are mixed to give the mixture of two colloidal sols, which was subjected to a multi-spin-coating process, which exhibits a morphology of dense grains and is united by grain boundaries [28]. On the other hand, a continuous porous morphology was obtained from zinc nitrate ($Zn(NO_3)_2{\cdot}6H_2O$, Sigma-Aldrich), aluminum nitrate ($Al(NO_3)_3x9H_2O$) and NH_3-H_2O, followed by the addition of a 1:1 (*v*/*v*) solution of NH_3, precipitation to pH 7 and drying at 100 °C and then at 800 °C [29].

A different ZnO/Al_2O_3 morphology with a "metallic foam" type morphology was obtained from a mixed suspension of Al_2O_3 and ZnO powders. Then, the stable mixed

suspension spray dried, and the resulting powder was first burned out at 500 °C for 4 h in air, and then sintered in flowing argon at 1400 °C for 2 h [30].

A morphology of the ZnO/Al_2O_3 composite similar to that obtained by our present method was observed using a solution method starting from the precursors ($Zn(CH_3COO)_2{\cdot}2H_2O$, Merck, 99.5%), urea, NH_2CONH_2 and bayerite powder, $Al(OH)_3$; in the presence of urea, the collar induced a precipitate, which was calcined at 400 °C [31].

The morphology of the Eu_2O_3/TiO_2 composite (see Figure S5a of Supplementary Materials) shows fractured and multiform cubohedrons joined in a disorderly manner. No SEM studies of this type of composite for the comparison of morphologies were found in the literature.

The morphology of the Eu_2O_3/Al_2O_3 composite (see Figure S5b of Supplementary Materials) is of the "metallic foam" type. No SEM studies of similar composites prepared using other methods for the comparison of morphologies were found in the literature.

4. Conclusions

The composites Au/SiO_2, Au/TiO_2, Au/Al_2O_3, ZnO/TiO_2, ZnO/TiO_2, ZnO/Al_2O_3 and Eu_2O_3/SiO_2, Eu_2O_3/TiO_2 and Eu_2O_3/Al_2O_3 were prepared in a single step, unlike another in a solution that involves at least two stages. The effect of the polymer precursors was investigated using the polymer Chitosan and Poly(styrene-co-4vinylpyridine), (PS-co-4-PVP) in the M/M_xL_y•Chitosan//$M'_xO'_y$ as well as M/M_xL_y•PS-co-4-PVP//$M'_xO'_y$ with $M'_xO'_y$ = SiO_2, TiO_2 and Al_2O_3. The nanocomposites were obtained in a single step, unlike another in solution that involves at least two stages. SiO_2 induces small and well-distributed Au nanoparticles inside the matrix, while TiO_2 and Al_2O_3 induce nanoparticles that are not well distributed rather than agglomerate Au nanoparticles inside both matrices.

In relation to morphology, SiO_2 and TiO_2 induce dense agglomerate grains of Au inside with varied forms, while for the Au inside Al_2O_3, a "some foam" 3D form was observed. Marked optical and photocatalytic effects of the Au, ZnO and Eu_2O_3 inside the SiO_2, TiO_2 and Al_2O_3 matrices are expected. Those experiments are in course.

Supplementary Materials: The following supporting information can be downloaded at: https://www.mdpi.com/article/10.3390/micro3030049/s1, Table S1: Experimental Details of the synthesis of the precursors 1-18.

Author Contributions: Conceptualization, supervision and funding acquisition, C.D.; methodology, O.C.-V.; formal analysis. and writing—original draft preparation, M.L.V. All authors have read and agreed to the published version of the manuscript.

Funding: This research was funded by the Fondecyt Project (1160241), which has finished acknowledged.

Data Availability Statement: Not applicable.

Acknowledgments: Miguel A. Laguna-Bercero is acknowledged for assisting with the HRTEM analysis using Servicio General de Apoyo a la Investigación (SAI, University of Zaragoza).

Conflicts of Interest: The authors declare no conflict of interest.

References

1. Kelly, K.L.; Coronado, E.; Zhao, L.L.; Schatz, G.C. The Optical Properties of Metal Nanoparticles: The Influence of Size, Shape, and Dielectric Environment. *J. Phys. Chem. B* **2003**, *107*, 668–677. [CrossRef]
2. Jensen, T.R.; Duval, M.L.; Kelly, K.L.; Lazarides, A.A.; Schatz, G.C.; Van Duye, R.P. Nanosphere Lithography: Effect of the External Dielectric Medium on the Surface Plasmon Resonance Spectrum of a Periodic Array of Silver Nanoparticles. *J. Phys. Chem. B* **1999**, *103*, 9846–9853. [CrossRef]
3. Armelao, L.; Barreca, D.; Bottaro, G.; Gasparotto, A.; Gross, S.; Maragno, C.; Tondello, E. Recent trends on nanocomposites based on Cu, Ag and Au clusters: A closer look. *Coord. Chem. Rev.* **2006**, *250*, 1294–1314. [CrossRef]
4. Walters, G.; Parkin, I.P. The incorporation of noble metal nanoparticles into host matrix thin films: Synthesis, characterization and applications. *J. Mater. Chem.* **2009**, *19*, 574–590. [CrossRef]
5. Matsuoka, J.; Yoshida, H.; Nasu, H.; Kamiya, K. Preparation of Gold Microcrystal-Doped TiO_2, ZrO_2 and Al_2O_3 Films Through Sol-Gel Process. *J. Sol-Gel Sci. Technol.* **1997**, *9*, 145–155. [CrossRef]

6. Prevel, B.; Palpant, B.; Lerme, J.; Pellarin, M.; Treilleux, M.; Saviot, L.; Duval, E.; Perez, A.; Broyer, M. Comparative analysis of optical properties of gold and silver clusters embedded in an alumina matrix. *Nanostructured Mater.* **1999**, *12*, 307–310. [CrossRef]
7. Epifani, M.; De, G.; Licciulli, A.; Vasanelli, L. Preparation of uniformly dispersed copper nanocluster doped silica glasses by the sol–gel process. *J. Mater. Chem.* **2001**, *11*, 3326–3332. [CrossRef]
8. Torrell, M.; Cunha, L.; Cavaleiro, A.; Alves, E.; Barradas, N.P.; Vaz, F. Functional and optical properties of Au: TiO_2 nanocomposite films: The influence of thermal annealing. *Appl. Surf. Sci.* **2010**, *256*, 6536–6542. [CrossRef]
9. Gonella, F.; Mattei, G.; Mazzoldi, P.; Battaglin, G.; Quaranta, A.; De, G.; Montecchi, M. Structural and optical properties of silver-doped zirconia and mixed zirconia-silica matrices obtained by sol-gel processing. *Chem. Mater.* **1999**, *11*, 814–821. [CrossRef]
10. Xu, L.; Cui, F.; Zhang, J.; Zhang, X.; Wang, Y.; Cui, T. A general autocatalytic route toward silica nanospheres with ultrasmall sized and well-dispersed metal oxide nanoparticles. *Nanoscale* **2018**, *10*, 9460–9465. [CrossRef]
11. Joshi, D.P.; Pant, G.; Arora, N.; Nainwal, S. Effect of solvents on morphology, magnetic and dielectric properties of (α-Fe_2O_3@SiO_2) core-shell nanoparticle. *Heliyon* **2017**, *3*, e00253. [CrossRef] [PubMed]
12. Chandra, P.; Doke, D.S.; Unbarkar, S.D.; Biradar, A.V. One-pot synthesis of ultrasmall MoO_3 nanoparticles supported on SiO_2, TiO_2, and ZrO_2 nanospheres: An efficient epoxidation catalyst. *J. Mater. Chem. A* **2014**, *2*, 19056–19060. [CrossRef]
13. Díaz, C.; Valenzuela, M.L.; Cifuentes-Vaca, O.; Segovia, M.; Laguna-Bercero, M.A. Incorporation of NiO into SiO_2, TiO_2, Al_2O_3, and $Na_{4.2}Ca_{2.8}(Si_6O_{18})$ Matrices: Medium Effect on the Optical Properties and Catalytic Degradation of Methylene Blue. *Nanomaterials* **2020**, *10*, 2470.
14. Díaz, C.; Valenzuela, M.L.; Soto, K.; Laguna-Bercero, M.A. Incorporation of Au and Ag Nanostructures Inside SiO_2. *J. Chin. Chem. Soc.* **2019**, *64*, 4502–4506. [CrossRef]
15. Díaz, C.; Valenzuela, M.L.; Segovia, M.; Correa, K.; De la Campa, R.; Soto, A.P. Solution, Solid-State Two Step Synthesis and Optical Properties of ZnO and SnO_2 Nanoparticles and Their Nanocomposites with SiO_2. *J. Clust. Sci.* **2018**, *29*, 251–266. [CrossRef]
16. Díaz, C.; Valenzuela, M.L.; Garcia, C.; de la Campa, R.; Soto, A.P. Solid-state synthesis of pure and doped lanthanide oxide nanomaterials by using polymer templates. Study of their luminescent properties. *Mater. Lett.* **2017**, *209*, 111–114. [CrossRef]
17. Díaz, C.; Valenzuela, M.L.; Cifuentes-Vaca, O.; Segovia, M.; Laguna-Bercero, M.A. Incorporation of Nanostructured ReO_3 in Silica Matrix and Their Activity Toward Photodegradation of Blue Methylene. *J. Inorg. Organomet. Polym. Mater.* **2020**, *30*, 1726–1734. [CrossRef]
18. Díaz, C.; Valenzuela, M.L.; Cifuentes-Vaca, O.; Segovia, M.; Laguna-Bercero, M.A. Iridium nanostructured metal oxide, its inclusion in silica matrix and their activity toward photodegradation of methylene blue. *Mater. Chem. Phys.* **2020**, *252*, 123276. [CrossRef]
19. Diaz, C.; Valenzuela, M.L.; Laguna-Bercero, M.A.; Mendoza, K.; Cartes, P. Solventless preparation of thoria, their inclusion inside SiO_2 and TiO_2, their luminescent properties and their photocataltytic behavior. *ACS Omega* **2021**, *6*, 9391–9400. [CrossRef]
20. Brugnerotto, J.; Lizardi, J.; Goycoolea, F.M.; Arguelles-Monal, W.; Desbrieres, J.; Rinaudo, M. An infrared investigation in relation with chitin and chitosan characterization. *Polymer* **2001**, *42*, 3569–3580. [CrossRef]
21. Armelao, L.; Barreca, D.; Gasparotto, A.; Pierangelo, E.; Tondello, E.; Stefano; Polizzi, S. Preparation of Gold Nanoparticles on Silica Substrate by Radio Frequency Sputtering. *J. Nanosci. Nanotechnol.* **2005**, *5*, 259–265. [CrossRef]
22. Liu, X.; Ding, B.; Zhu, Y.; Wang, T.; Chen, B.; Shao, Y.; Chen, M.; Zheng, P.; Zhao, Y.; Qian, H. Facile synthesis of the SiO_2/Au hybrid microspheres for excellent catalytic performance. *J. Mater. Res.* **2014**, *29*, 1417–1423. [CrossRef]
23. Wang, W.; Meng, Z.; Zhang, Q.; Jia, W.; Xi, K. Synthesis of stable Au–SiO_2 composite nanospheres with good catalytic activity and SERS effect. *J. Colloid Interface Sci.* **2014**, *418*, 1–7. [CrossRef]
24. Zhou, M.; Zhang, J.; Cheng, B.; Yu, H. Enhancement of Visible-Light Photocatalytic Activity of Mesoporous Au-TiO_2 Nanocomposites by Surface Plasmon Resonance. *Int. J. Photoenergy* **2012**, *2012*, 532843. [CrossRef]
25. Yang, X.; Wu, X.; Lia, J.; Liu, Y. TiO_2–Au composite nanofibers for photocatalytic hydrogen evolution. *RSC Adv.* **2019**, *9*, 29097–29104. [CrossRef]
26. Eskandari, M.J.; Shafyei, A.; Karimzadeh, F. One-step fabrication of Au@Al_2O_3 core-shell nanoparticles by continuous wave fiber laser ablation of thin gold layer on aluminum surface. *Struct. Opt. Prop. Opt. Laser Technol.* **2020**, *126*, 106066. [CrossRef]
27. Rao, W.; Wang, D.; Kups, T.; Baradács, E.; Parditka, B.; Erdélyi, Z.; Schaaf, P. Nanoporous Gold Nanoparticles and Au/Al_2O_3 Hybrid Nanoparticles with Large Tunability of Plasmonic Properties. *ACS Appl. Mater. Interfaces* **2017**, *9*, 6273–6281. [CrossRef] [PubMed]
28. Tang, Y.; Xu, X.; Han, S.; Cai, C.; Du, H.; Zhu, H.; Zu, X.; Fu, Y.Q. ZnO-Al_2O_3 nanocomposite as a sensitive layer for high performance surface acoustic wave H_2S gas sensor with enhanced elastic loading effect. *Sens. Actuators B Chem.* **2020**, *304*, 127395. [CrossRef]
29. Yadav, S.; Mittal, A.; Sharma, S.; Kumari, K.; Chauhan, N.S.; Kumar, N. Low temperature synthesized ZnO/Al_2O_3 nanocomposites for photocatalytic and antibacterial applications. *Semicond. Sci. Technol.* **2020**, *35*, 055008. [CrossRef]

30. Bouhamed, H.; Baklouti, S. Synthesis and characterization of Al2O3/ZnO nanocomposite by pressureless sintering. *Powder Technol.* **2014**, *264*, 278–290. [CrossRef]
31. Tajizadegana, H.; Jafari, M.; Rashidzadehb, M.; Saffar-Teluri, A. A high activity adsorbent of ZnO–Al_2O_3 nanocomposite particles: Synthesis, characterization and dye removal efficiency. *Appl. Surf. Sci.* **2013**, *276*, 317–322. [CrossRef]